Cancer Letters 507 (2021) 80–88

Contents lists available at ScienceDirect

Cancer Letters

journal homepage: www.elsevier.com/locate/canlet

Expression of activated VEGFR2 by R1051Q mutation alters the energy metabolism of Sk-Mel-31 melanoma cells by increasing glutamine dependence

Elisabetta Grillo [a,*], Michela Corsini [a], Cosetta Ravelli [a], Luca Zammataro [b], Marina Bacci [c], Andrea Morandi [c], Eugenio Monti [a], Marco Presta [a], Stefania Mitola [a,**]

[a] Department of Molecular and Translational Medicine, University of Brescia, Brescia, 25123, Italy
[b] Department of Obstetrics, Gynecology and Reproductive Sciences, Yale School of Medicine, New Haven, CT, 06510, USA
[c] Department of Experimental and Clinical Biomedical Sciences, University of Florence, Florence, 50134, Italy

ARTICLE INFO

Keywords:
VEGFR2
Mutation
Energy metabolism
Glutamine

ABSTRACT

Vascular endothelial growth factor receptor 2 (VEGFR2) activating mutations are emerging as important oncogenic driver events. Understanding the biological implications of such mutations may help to pinpoint novel therapeutic targets. Here we show that activated VEGFR2 *via* the pro-oncogenic R1051Q mutation induces relevant metabolic changes in melanoma cells. The expression of VEGFR2^{R1051Q} leads to higher energy metabolism and ATP production compared to control cells expressing VEGFR2^{WT}. Furthermore, activated VEGFR2^{R1051Q} augments the dependence on glutamine (Gln) of melanoma cells, thus increasing Gln uptake and their sensitivity to Gln deprivation and to inhibitors of glutaminase, the enzyme initiating Gln metabolism by cells. Overall, these results highlight Gln addiction as a metabolic vulnerability of tumors harboring the activating VEGFR2^{R1051Q} mutation and suggest novel therapeutic approaches for those patients harboring activating mutations of VEGFR2.

1. Introduction

Activation of receptor tyrosine kinases (RTKs) or activation of their downstream intracellular effectors by point mutations or gene amplifications are typical hallmarks of cancer [1]. However, targeting these alterations has been only partially successful in clinical oncology. New therapeutic opportunities are now emerging and direct attention to the metabolic features of cancer cells that are secondary to RTK alterations. Similarly, targeting metabolic adaptations following KRAS mutations is considered a promising approach to block the growth of KRAS-mutated tumors [2]. It is therefore crucial to obtain a deep understanding of the biological consequences of RTK alterations in order to reveal novel therapeutic windows of intervention.

Metabolic rewiring is central to tumorigenesis. Various metabolic adaptations, including increased energy metabolism (i.e. glycolysis and oxidative phosphorylation, OXPHOS), are functional to sustain the higher energetic and biosynthetic demands of tumor cells [3]. RTKs govern cell metabolism, controlling the uptake of nutrients and regulate the function of key enzymes, for example PKM2, thus directing different carbon fuels into catabolic and anabolic pathways. Activation of RTKs promotes glycolysis, OXPHOS, and nucleotide and lipid biosynthesis, through the activation of the PI3K/Akt or Ras/B-Raf/MEK signaling pathways. In addition, they regulate utilization of glucose (Glc) and amino acids to sustain biosynthesis and TCA anaplerosis *via* Myc and HIF transcription factors and mTOR kinase [4]. Recently, metabolic perturbations associated with oncogenic activation of RTKs have been described. EGFR branches glycolysis to the serine synthesis, to synthetize nucleotides and maintain redox balance, while FGFR activation recycles lactate to sustain energy production *via* OXPHOS [5].

Vascular endothelial growth factor receptor 2 (VEGFR2) is a classical RTK expressed in tumor cells, including gastric and ovarian cancer and melanoma, where it regulates cell proliferation, motility, and stemness [6–11], thus representing an attractive therapeutic target. Several VEGFR2-selective tyrosine kinase inhibitors (TKi), including sorafenib, sunitinib and apatanib, are used by oncologists or in clinical trials for the treatment of various tumors ([12]; ClinicalTrials.gov). However, poor

* Corresponding author. Department of Molecular and Translational Medicine, University of Brescia, Via Branze 39, Brescia, 25123, Italy.
** Corresponding author. Department of Molecular and Translational Medicine, University of Brescia, Via Branze 39, Brescia, 25123, Italy.
E-mail addresses: elisabetta.grillo@unibs.it (E. Grillo), stefania.mitola@unibs.it (S. Mitola).

https://doi.org/10.1016/j.canlet.2021.03.007
Received 30 December 2020; Received in revised form 3 March 2021; Accepted 5 March 2021
Available online 17 March 2021

response and resistance often occur, manifesting the need for a better stratification of patients to receive anti-VEGFR2 treatment and for the identification of novel pharmacological strategies.

VEGFR2 mutations are emerging as important oncogenic driver events and/or predictors of drug response in various cancer types. Several point mutations of VEGFR2 are associated with poor prognosis and/or altered response to targeted therapeutics. Among them, the mutations D717V, G800D/R, G843D, S925F, R1022Q, R1032Q, R1051Q and S1100F promote tumor growth in murine models [13,14], L840F substitution induces therapy resistance in colon cancer patients [14], while D717V, R961W, R1032Q, R1051Q and A1065T mutations are associated with better response to TKi [13,15–17]. At the functional level, R1032Q and S1100F substitutions entail a loss-of-function [18], while the mutations N717V, R1051Q, D1052N and A1065T promote the auto phosphorylation of VEGFR2, suggesting that they are activating mutations [13,15]. On these bases, screening for VEGFR2 alterations may help to stratify patients to receive anti-VEGFR2 drugs. Despite this, our understanding of the biology of VEGFR2 mutations is poor, compared to other RTKs.

Among all tumor types, melanoma depends on autocrine VEGF/VEGFR2 signaling [9], and the axis VEGF/VEGFR2 became a therapeutic target. Unfortunately, clinical evidence showed that targeting this axis elicits only moderate effects on patient outcome, pointing that new approaches are urgently required.

We recently identified the activating R1051Q mutation of VEGFR2 that creates a ligand-independent active receptor which drives melanoma progression [13]. Here we sought to investigate the metabolic rewiring associated with this VEGFR2 activating mutation in melanoma to identify potential new therapeutic targets. Functional analyses revealed that hyper-activated VEGFR2 leads to relevant metabolic changes, with increased glycolysis and OXPHOS, resulting in enhanced glutamine (Gln) consumption and dependency. Our data describe for the first time Gln addiction as a metabolic vulnerability of melanoma cells harboring VEGFR2^{R1051Q} mutation. Relevant to this point, recent work has shown that a subset of melanomas, classified as high-OXPHOS, can be effectively targeted with the glutaminase inhibitor BPTES, encouraging the development of therapeutic strategies directed against mitochondria [19]. Our data further support the hypothesis that metabolism-targeted drugs may be combined with classical chemotherapy to treat VEGFR2-mutated melanoma.

2. Material and methods

Cell cultures. Human melanoma a-melanotic Sk-Mel-31 cells (expressing wild-type B-Raf, N-Ras and VEGFR2) were obtained from the Memorial Sloan Kettering Cancer Center and were grown in RPMI (ThermoFisher), supplemented with 10% FCS (Invitrogen), non-essential amino-acids (ThermoFisher) and penicillin/streptomycin (ThermoFisher) (growth medium). Cells were stably transfected with pBE_hVEGFR2 [NM_002253.2] or pBE_hVEGFR2^{R1051Q} plasmids (generated as described in Ref. [13]) to obtain Sk-Mel-31-VEGFR2^{WT} or Sk-Mel-31-VEGFR2^{R1051Q} cell lines. Transfected cell lines were maintained in 0.5 mg/mL geneticin (ThermoFisher). Two independent transfections resulted in similar levels of VEGFR2 expression and similar biological phenotype. Cells were regularly checked for Mycoplasma contamination by PCR.

Antibody array and Western blot analyses. Total lysates (50 μg) from Sk-Mel-31-VEGFR2^{WT} or Sk-Mel-31-VEGFR2^{R1051Q} cells were separated by SDS-PAGE and probed with specific antibodies. Chemiluminescent signal was acquired by ChemiDoc™ Imaging System (BioRad) [20]. For mitochondrial complexes, lysates were run under non-reducing conditions. Alternatively, 500 μg of total lysates were incubated with the Human Phospho-Kinase Antibody Array (R&D Systems) according to manufacturer's instructions. Chemiluminescent signal was quantified by the open source ImageJ software (https://imagej.nih.gov/ij/) and normalized on reference spots. Background correction was achieved by the "subtract background" command [21].

RT-PCR array. Two μg of total RNA were retro-transcribed with rtStar™ First-Strand cDNA Synthesis Kit (Arraystar Inc, Rockville, MD - USA). The expression of 373 transcripts encoding the enzymes or proteins involved in cell metabolism was measured by NuRNA™ Central Metabolism PCR array (Arraystar Inc) using SYBR® Green qPCR Master Mix (Arraystar Inc) according to manufacturer's instructions. Fold change of $2^{-\Delta\Delta Ct}$ was calculated using *human_18S* RNA as housekeeping and Sk-Mel-31-VEGFR2^{WT} cells as control. Gene symbols are derived from the Human gene nomenclature committee (https://www.genenames.org).

Bioinformatic analyses. Differentially expressed genes in SK-Mel-31-VEGFR2^{R1051Q} cells *versus* SK-Mel-31-VEGFR2^{WT} cells ($\leq$0.5 or $\geq$1.5 fold change) identified by the PCR array were analyzed by the gene list enrichment analysis tool Enrichr (https://maayanlab.cloud/Enrichr/) [22,23] using the MSigDB hallmark 2020 library. Enriched pathways are sorted by the combined score ranking. Combined score is computed by taking the log of the p-value from the Fisher exact test and multiplying that by the z-score of the deviation from the expected rank.

Metabolic analyses. 4×10^4 cells were seeded in Seahorse XFe24 culture plates (Agilent Technologies) and incubated in a CO_2 incubator at 37 °C. Linifanib (Selleckchem) or vehicle (DMSO) were added when indicated. After 18 h, cells were checked by microscope for confluence and the medium was replaced with Agilent Seahorse XF base medium DMEM (pH 7.4) added with 10 mM Glc (Merck Millipore), 1 mM sodium pyruvate (ThermoFisher) and 2 mM Gln (ThermoFisher). Cells were incubated for 1 h at 37 °C and subjected to Seahorse analyses as described in Ref. [24]. Proton efflux rate (PER), oxygen consumption rate (OCR) and extracellular acidification rate (ECAR) measurements were performed at 6 min intervals (2 min mixing, 2 min waiting and 2 min measuring) using a Seahorse XFe24 Extracellular Flux Analyzer (XFe Wave software). Seahorse XF Glycolytic Rate Assay Kit, Seahorse XF Cell Mito Stress Test Kit and Seahorse XF Mito Fuel Flex Test Kit (Agilent) were employed to measure glycolytic activity, mitochondrial activity and mitochondrial fuel usage respectively following manufacturer's instructions. All indicated parameters were calculated using the Seahorse Report Generator (Agilent). At the end of each experiment cells were lysed and total protein amount was calculated by Bradford assay (BioRad). PER, OCR and ECAR data were normalized on total protein micrograms and are expressed as pmol/min/μg or mpH/min/μg, respectively.

Real-time measurement of ATP production was performed on 1×10^3 cells in growth medium with ATP Determination Kit (Molecular Probes) following manufacturer's instructions. Bioluminescent signal was measured with EnSight Multimode Plate Reader (PerkinElmer).

^{14}C-Gln uptake. Radioactive assay was run as previously described [25]. Briefly, 1×10^5 Sk-Mel-31-VEGFR2^{WT} and Sk-Mel-31-VEGFR2^{R1051Q} cells were maintained in growth medium. Prior to the analysis, cells were gently washed with PBS and medium was replaced with uptake buffer solution (140 mmol/L NaCl, 20 mM HEPES/Na, 2.5 mM $MgSO_4$, 1 mM $CaCl_2$, and 5 mM KCl, pH 7.4) containing 0.05 μCi/mL uniformly (U) radiolabeled [U–14C] Gln (PerkinElmer) for 15 min. Cells were subsequently washed for three times with PBS and lysed with 0.1 M NaOH. Samples were collected into a scintillation vial and counted on the scintillation counter. The radioactive signal was normalized on total protein content.

Cell proliferation. 6×10^3 cells/cm^2 were cultured in growth medium in the absence or the presence of indicated nutrients (Glc, Gln) or antimycin A, CB-839 or 968 inhibitors (Selleckchem) for 6 days. Medium was changed every second day. Cell number was evaluated by cell counting or by crystal violet colorimetric assay (OD at 595 nm).

Statistical analyses. Statistical analyses were performed using Prism 6 (GraphPad Software). Student's *t*-test for unpaired data (2-tailed) was used to test the probability of significant differences between two groups of samples. For more than two groups of samples data were analyzed with a one-way ANOVA and corrected by the Dunnett's multiple

comparisons test. Differences were considered significant when $p < 0.05$, unless otherwise specified.

3. Results

3.1. The expression of VEGFR2^{R1051Q} potentiates the PI3K/Akt/mTOR signaling pathway in melanoma cells

In a previous report, we demonstrated that the expression of VEGFR2^{R1051Q} in Sk-Mel-31 human melanoma cells leads to the hyper-activation of the PI3K/Akt pathway in tumor xenografts in mice [13]. To better understand the pro-tumorigenic molecular signaling modulated by the expression of activated VEGFR2 by R1051Q mutation in Sk-Mel-31 cells, we performed a phospho-kinase antibody array analysis of the cell extracts of VEGFR2^{R1051Q} transfectants. Sk-Mel-31 cells transfected with wild-type VEGFR2 (VEGFR2^{WT}) were used as control to exclude the effects consequent to the mere VEGFR2 overexpression (Fig. 1A). Of note, VEGFR2^{WT} expression did not have a significant impact on Sk-Mel-31 cell behavior, when compared to parental cells (data not shown). As anticipated, the expression of VEGFR2^{R1051Q} increases the phosphorylation of various intracellular kinases. In keeping with our previous *in vivo* observations, Sk-Mel-31-VEGFR2^{R1051Q} cells display a hyper-activated PI3K/Akt/mTOR signaling pathway with increased levels of phospho-Akt and its targets phospho-GSK-3α/β, phospho-AMPKα, phospho-CREB, phospho-p70 S6 kinase and phospho-WNK (Fig. 1B).

The prominent role of the PI3K/Akt/mTOR pathway in the regulation of cell metabolism [26] prompted us to investigate the impact of VEGFR2 activation by R1051Q mutation on metabolic pathways in Sk-Mel-31 cells. In the first instance, we analyzed by NuRNA™ Central Metabolism PCR array the expression levels of 373 genes encoding enzymes and proteins involved in cell metabolism (Fig. 1C). A total of 94 genes were differentially expressed in VEGFR2^{R1051Q} transfectants when compared to VEGFR2^{WT} cells, defined as genes showing a drop out of $\leq$0.5 or $\geq$1.5 fold change (Fig. 1D, top 10 up-/down-regulated genes are shown; full list in Supplementary Table 1). To understand the mechanism by which VEGFR2^{R1051Q} alters tumor metabolism, gene set enrichment analysis (GSEA) of PCR array data was performed by using MSigDB library and Enrichr tool [22,23]. The results showed significant enrichment of the OXPHOS pathway, with upregulated *PDHX*, *CPT1A*, *ACAA2*, *SDHC*, *ACAT1*, *PDP1*, *LDHA*, *PD4*, *PGDH*, *DLAT* and down-regulated *ECH1*, *GOT2*, *ETFA*, *GLUD1*, *NNT* genes. GSEA analysis revealed also the alteration of fatty acid (FA) metabolism, cholesterol homeostasis and glycolytic pathways, the latter characterized by the upregulation of *GOT1*, *AK3*, *LDHA*, *SLC16A3*, *SDHC* and the down-regulation of *GOT2*, *PFKP*, *PDK3* genes (Fig. 1D-E; Supplementary Table 2). Remarkably, the mTORC1 signaling pathway was also enriched, further confirming the hyper-activation of the PI3K/Akt/mTOR pathway in Sk-Mel-31-VEGFR2^{R1051Q} cells (Fig. 1E and F).

3.2. Glycolysis is enhanced in VEGFR2^{R1051Q} expressing melanoma cells

To elucidate how mutated VEGFR2^{R1051Q} rewires the metabolic pathways in melanoma cells, we analyzed the energy metabolism of Sk-Mel-31-VEGFR2^{WT} and Sk-Mel-31-VEGFR2^{R1051Q} cells by Seahorse technology. First, we took advantage of the Seahorse Glycolytic Rate Assay which measures the proton efflux rate (PER) as a readout of the cellular glycolytic activity-dependent (gPER) or mitochondrial/CO_2-dependent (mPER) medium acidification. At the basal state, melanoma cells expressing VEGFR2^{R1051Q} increase their overall PER (Fig. 2A and B) when compared to cells expressing the wild-type receptor as a result of an increase in both gPER and mPER (Fig. 2B). These observations indicate that the expression of mutated VEGFR2 in melanoma cells increases the channeling of pyruvate into lactate and that, besides glycolysis, also OXPHOS is enhanced, as suggested by increased mPER. In addition, to assess the maximal glycolytic capacity of the two cell types, PER was measured upon OXPHOS inhibition by antimycin A/rotenone treatment. Under these experimental conditions, Sk-Mel-31-VEGFR2^{R1051Q} cells displayed a maximal glycolytic activity (Max gPER) significantly higher as compared to Sk-Mel-31-VEGFR2^{WT} cells (Fig. 2C).

3.3. VEGFR2^{R1051Q} expression increases oxidative phosphorylation

We further analyzed the oxygen consumption rate (OCR), an index of OXPHOS, in Sk-Mel-31-VEGFR2^{R1051Q} and Sk-Mel-31-VEGFR2^{WT} cells by Seahorse Mito-Stress Test. As shown in Fig. 3A, VEGFR2^{R1051Q} expression leads to higher basal OXPHOS. Also, ATP-linked respiration, measured following administration of the ATP synthase inhibitor oligomycin, was higher in Sk-Mel-31-VEGFR2^{R1051Q} cells, as demonstrated by the higher extent of OCR reduction. Next, the maximal OCR activity, measured following the administration of the protonophore uncoupler FCCP, was found significantly higher in Sk-Mel-31-VEGFR2^{R1051Q} cells as compared to Sk-Mel-31-VEGFR2^{WT} cells. Finally, the spare respiratory capacity, calculated as the difference between maximal and basal respiration rate, is increased in Sk-Mel-31-VEGFR2^{R1051Q} mutants. However, the proton leak, that is the difference between oligomycin inhibited OCR and rotenone/antimycin A (Rot/Ant-A) inhibited OCR, and non-mitochondrial respiration, measured as Rot/Ant-A inhibited OCR, do not differ in the two sublines. Moreover, the Mito-Stress test confirmed that the basal glycolysis is increased in Sk-Mel-31-VEGFR2^{R1051Q} cells compared to Sk-Mel-31-VEGFR2^{WT} as shown by the higher levels of extracellular acidification rate (ECAR) (Fig. 3A and B). In keeping with these data, the amount of ATP production was higher in VEGFR2^{R1051Q} transfectants when compared to control cells (Fig. 3C). These results confirmed GSEA results (shown in Fig. 1E and F) and indicate that constitutively active VEGFR2 signaling leads to increased oxidative metabolism, in the presence of active glycolysis.

Previous observations had shown that the R1051Q mutation increases the sensitivity of Sk-Mel-31-VEGFR2^{R1051Q} cells to the VEGFR2-targeted TKi Linifanib. Indeed, Linifanib selectively blocks the growth of tumors originating from Sk-Mel-31-VEGFR2^{R1051Q} cells while exerting no effect on Sk-Mel-31-VEGFR2^{WT} cells [13]. As expected, Linifanib induces a potent and dose-dependent decrease of basal and maximal OCR in melanoma cells expressing VEGFR2^{R1051Q}, while negligible effects were observed in Linifanib-treated Sk-Mel-31-VEGFR2^{WT} cells (Fig. 3D and E). These data confirm that the metabolic rewiring occurring in Sk-Mel-31-VEGFR2^{R1051Q} cells directly depends on the intracellular signaling downstream to mutated VEGFR2, and further confirm that, although overexpressed, VEGFR2^{WT} is not active in Sk-Mel-31-VEGFR2^{WT} cells. Remarkably, both cell lines express similar levels of electron transport chain elements, ruling out the possibility that the altered mitochondrial metabolism results from differences in the mitochondrial mass (Fig. 3F). Despite their different OXPHOS activity, the two cell lines display comparable sensitivity to Antimycin A administration in terms of survival (Fig. 3G).

3.4. VEGFR2^{R1051Q} expression increases melanoma cell dependency on glutamine

Oncogenic alterations often lead to altered metabolic reliance on carbon sources in cancer cells. This has allowed to detect druggable metabolic vulnerabilities for many cancer types [5]. To investigate whether the expression of oncogenic VEGFR2^{R1051Q} influences the reliance on the three major carbon sources, we measured the specific contribution of fatty acids (FA), Glc and Gln to mitochondrial respiration by the Mito Fuel Flex Test. In a first set of experiments, we estimated cell dependency on specific carbon sources by measuring the basal OCR before and after addition of the specific inhibitors of the three target pathways etomoxir, UK5099 or BPTES, respectively. Sk-Mel-31-VEGFR2^{WT} and Sk-Mel-31-VEGFR2^{R1051Q} cells exhibit comparable metabolic dependence on FA and Glc. On the other hand, the expression

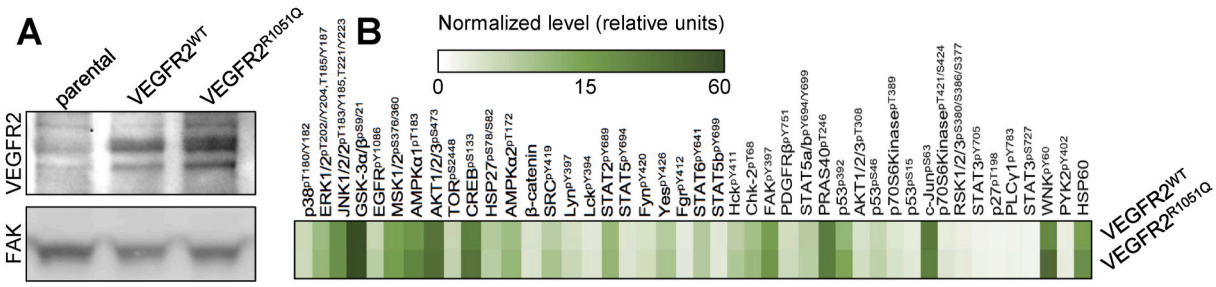

D

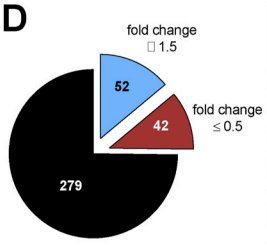

Gene	Metabolic function	Fold change (log2)
LDHA	Pyruvate metabolism	13.93
AMPD3	Purine salvage	5.57
AHCYL2	L-homocysteine biosynthesis	4.90
CPT1A	Fatty acid beta-oxidation	4.19
GUCY1A2	Purine metabolism	3.81
PDHX	Pyruvate metabolism/amino acid metabolism	3.77
ACAD10	Mitochondrial Fatty Acid Beta-Oxidation	3.53
UCKL1	Pyrimidine salvage	2.88
GLS2	Glutamate and glutamine metabolism	2.80
UPP1	Pyrimidine salvage/catabolism	2.56

Gene	Metabolic function	Fold change (log2)
SDHAF4	Tricarboxylic acid cycle/Electron transport chain	-35.04
SUCLG2	Tricarboxylic acid cycle	-31.33
PKM2	Glycolysis	-13.51
ADSS	Purine biosynthesis	-10.85
ECH1	Fatty acid beta-oxidation	-6.38
L2HGDH	2-oxoglutarate metabolism	-4.00
GOT2	Gluconeogenesis/amino acid metabolism	-3.13
SLC1A2	Glutamate transporter	-3.06
SLC1A3	Glutamate transporter	-3.04
PPAT	Purine biosynthesis	-2.93

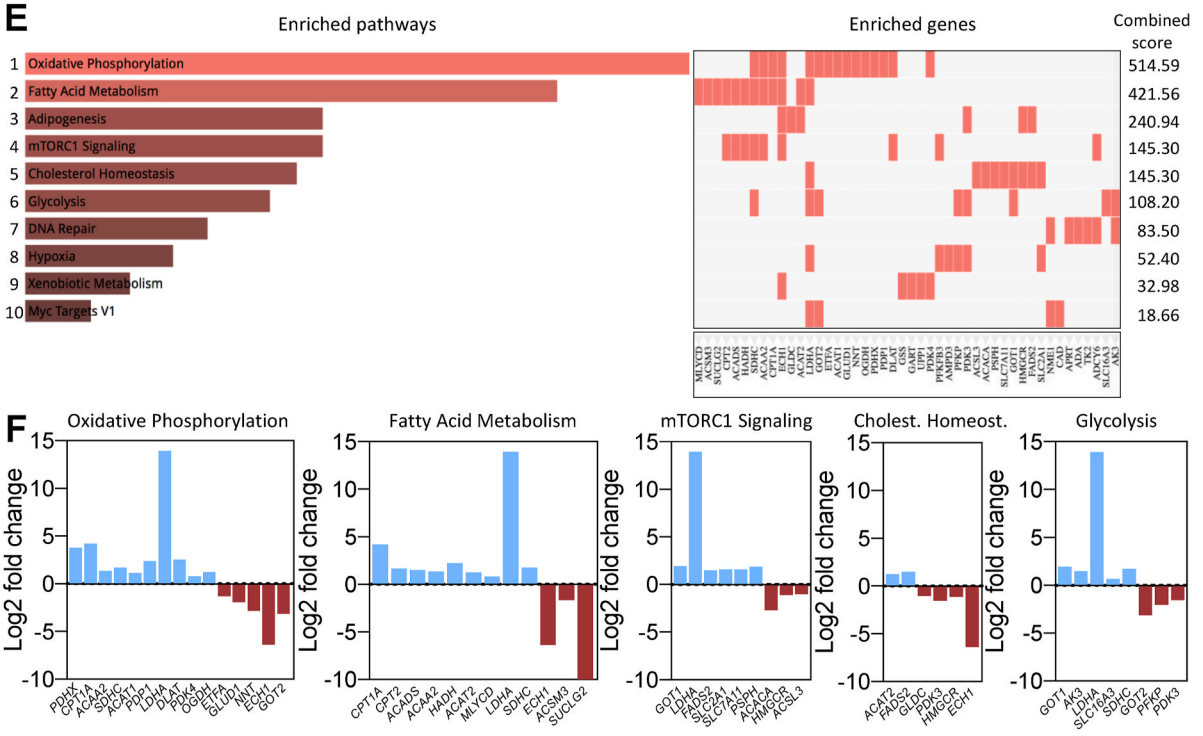

Fig. 1. Impact of VEGFR2^{R1051Q} expression on melanoma cell metabolism. A: Western blot analysis of total VEGFR2 levels in parental and transfected Sk-Mel-31-VEGFR2^{WT} and Sk-Mel-31-VEGFR2^{R1051Q} cells. **B:** Human Phospho-Kinase Antibody Array on Sk-Mel-31-VEGFR2^{WT} and Sk-Mel-31-VEGFR2^{R1051Q} total cell lysates. The heatmap shows the color-coded normalized protein levels of all detected proteins. One representative experiment out of three independent replicates that provided similar results is shown. **C:** schematic of metabolic pathway enrichment analysis of dropout genes from NuRNA™ Central Metabolism PCR array in Sk-Mel-31-VEGFR2^{R1051Q} *versus* Sk-Mel-31-VEGFR2^{WT} cells (created with BioRender.com). **D:** Lists of top 10 drop out genes [fold change ≤0.5 (red) or ≥1.5 (blue)] in Sk-Mel-31-VEGFR2^{R1051Q} *versus* Sk-Mel-31-VEGFR2^{WT} cells sorted by Log2 fold change. **E:** MSigDB pathway enrichment analysis using Enrichr software. **F:** Bar graphs depicting individual Log2 fold change for each gene belonging to enriched gene sets in Sk-Mel-31-VEGFR2^{R1051Q} *versus* Sk-Mel-31-VEGFR2^{WT} cells. (For interpretation of the references to color in this figure legend, the reader is referred to the Web version of this article.)

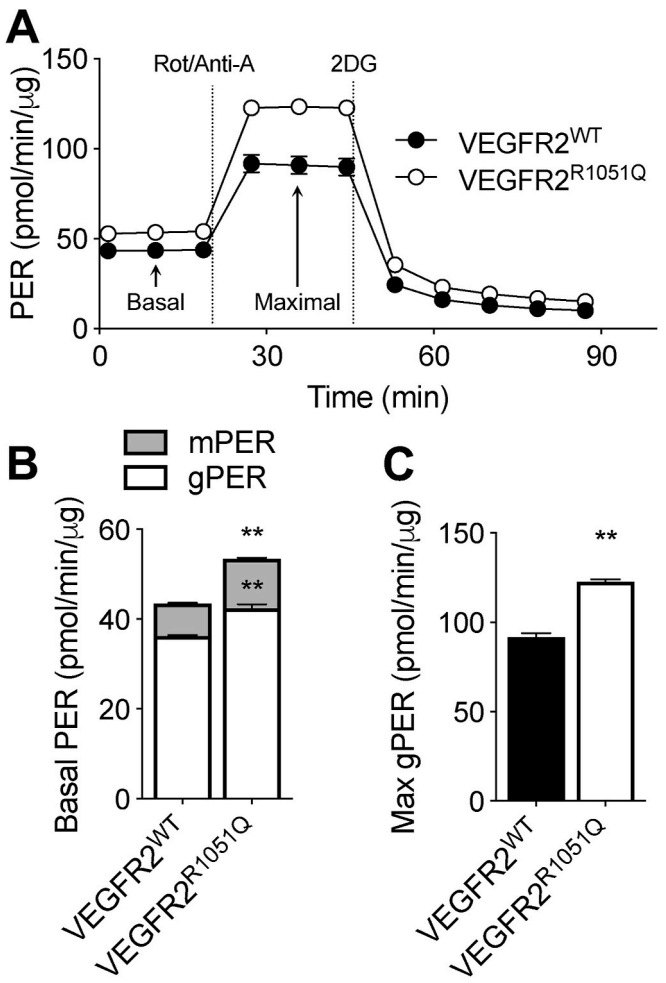

Fig. 2. Glycolysis in melanoma cells expressing VEGFR2^{R1051Q}. Seahorse Glycolytic Rate Assay performed on Sk-Mel-31-VEGFR2^{WT} and Sk-Mel-31-VEGFR2^{R1051Q} cells. Cells were seeded in Seahorse XFe24 culture plates and incubated in CO_2 incubator at 37 °C. After 18 h, the medium was replaced with Agilent Seahorse XF base medium DMEM (pH 7.4) added with 10 mM Glc, 1 mM sodium pyruvate and 2 mM Gln. Cells were incubated for 1 h at 37 °C before performing Seahorse measurements. Proton efflux rate (PER) was measured over time before and after sequential addition of 0.5 μM Rotenone/Antimycin-A (Rot/Anti-A) and 50 mM 2-deoxy-D-glucose (2DG). **A**: PER over time. **B:** basal glycolytic and mitochondrial PER (gPER, mPER). **C:** maximal glycolytic PER. Glycolytic and mitochondrial PER were calculated using the Seahorse Report Generator. Data are the mean ± SEM of three technical replicates in one representative experiment out of three independent measurements that provided similar results. **, $p < 0.01$, Student's *t*-test *versus* Sk-Mel-31-VEGFR2^{WT}.

of VEGFR2^{R1051Q} leads to a significant increase of the metabolic dependence on Gln (Fig. 4A, white bars), pointing to Gln supply as a metabolic requirement for sustaining energy production and, possibly, cell growth in melanoma cells expressing oncogenic VEGFR2^{R1051Q}.

Next, we analyzed the maximal ability of Sk-Mel-31 cells to oxidize a specific substrate (termed "capacity") by measuring the basal OCR before and after the addition of selective inhibitors of the other two pathways (i.e. UK5099/BPTES, BPTES/etomoxir, UK5099/etomoxir). While the capacity for FA and Gln were similar in both cell lines, Sk-Mel-31-VEGFR2^{R1051Q} cells exhibit a reduced capacity for Glc (Fig. 4A). To better understand this metabolic behavior, we analyzed the metabolic flexibility, that is the relative ability of cells to switch OXPHOS from one fuel to another, calculated as the difference between capacity and dependency. Results demonstrated that Sk-Mel-31-VEGFR2^{R1051Q} cells have a lower relative flexibility than cells expressing the wild-type receptor for all the three nutrients (Fig. 4A, grey bars), most probably because they oxidize the substrates at a rate which is close to their maximum potential already at the basal state. In addition, the maximal Glc usage is reduced in Sk-Mel-31-VEGFR2^{R1051Q} cells, possibly due to increased usage of Gln.

Altogether, these results suggest that melanoma cells expressing the activated VEGFR2^{R1051Q} become metabolically addicted to Gln. Accordingly, the uptake of ^{14}C-Gln is significantly increased in Sk-Mel-31-VEGFR2^{R1051Q} cells (Fig. 4B). Moreover, Gln deprivation strongly hampers the basal OCR and slows down the cell proliferation of Sk-Mel-31-VEGFR2^{R1051Q} cells, exerting instead much milder effects on the control cells. Under the same experimental conditions, Glc deprivation selectively reduces the basal OCR of cells expressing mutated VEGFR2^{R1051Q}, suggesting that a significant amount of Glc is oxidized to pyruvate to fuel cellular respiration in these cells. However, Glc withdrawal completely abrogates the ECAR and stops the growth of Sk-Mel-31 cells regardless if they express wild-type or mutant VEGFR2. This suggests that VEGFR2^{R1051Q} does not further increase the already high glycolytic addiction of Sk-Mel-31 cells (Fig. 4C–E). In accordance with Gln deprivation experiments, treatments with glutaminase-1 (GLS-1) specific inhibitor CB-839 or the pan GLS-1/2 inhibitor 968 reduce with higher potency the growth of VEGFR2^{R1051Q} cells than that of Sk-Mel-31-VEGFR2^{WT} cells (Fig. 4F and G). On these bases, we concluded that the activation of VEGFR2 *via* the R1051Q mutation induces strong metabolic perturbations, increasing the uptake, consumption of and dependence on Gln in melanoma cells.

4. Discussion

One hallmark of fast-growing cancer cells is a high glycolytic flux with lactate production even in the presence of adequate amounts of oxygen, defined as "Warburg effect". Besides, cancer cells can rely also on OXPHOS, even when glycolysis is highly active [27]. The metabolic flexibility of cancer cells guarantees fast adaptation to changes in nutrient availability [28].

Oncogenes orchestrate metabolic reprogramming that sustains malignant transformation and tumor progression [3,27]. Recently, RTK alterations have been associated with various metabolic adaptations in cancer cells. For example, the oncogenic activation of EGFR branches glycolysis to the serine synthesis to synthetize nucleotides and maintain redox balance, while FGFR activation recycles lactate to sustain energy production *via* OXPHOS [5]. As concerns VEGFR2, little is known, except that it regulates Glc uptake and lactate production in ovarian and colorectal cancer [29,30], while it triggers mitochondrial biogenesis in chemotherapy-exposed acute myeloid leukemia cells [31].

Here we exploited the mutation R1051Q of VEGFR2 as a model of aberrantly activated VEGFR2. This alteration has been recently characterized in our group as a gain-of-function mutation of the receptor. Mutated VEGFR2^{R1051Q} is active even in the absence of ligands and promotes tumor growth [13]. Based on the evidence that VEGFR2^{R1051Q} stimulates the PI3K/Akt/mTOR pathway *in vivo*, in the present study we investigated more in depth the metabolic changes occurring in melanoma cells when mutated VEGFR2^{R1051Q} is expressed. In accordance with the central role of the PI3K/Akt/mTOR pathway in metabolic control [32], oncogenic VEGFR2^{R1051Q} induces significant metabolic changes, including increased glycolysis and OXPHOS.

Melanin regulates the metabolic behavior of melanoma cells [33]. However, Sk-Mel-31 cells are a-melanotic [34] and RT-PCR analysis failed to demonstrate the presence of *TYR* transcripts in both parental and VEGFR2 transfectants (data not shown), ruling out the possibility that melanin levels may affect our observations. Future studies will unveil possible interactions between VEGFR2 signaling and melanin production in terms of metabolic adaptations.

VEGF signaling in endothelial cells increases glycolysis by inducing *GLUT1* and the glycolytic enzyme 6-phosphofructo-2-kinase/fructose-2,6-bisphosphatase-3 (*PFKFB3*) [35,36]. Similarly, GSEA showed

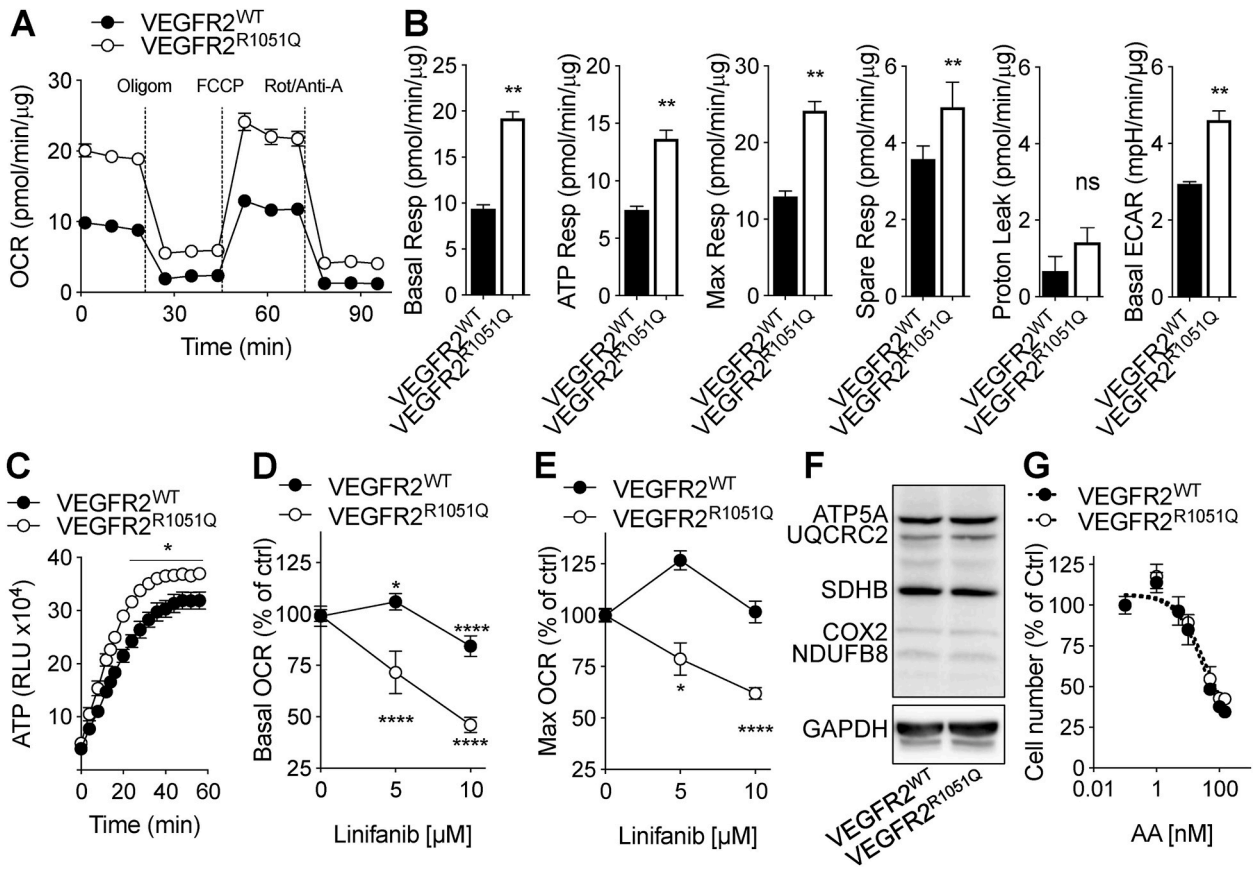

Fig. 3. OXPHOS in melanoma cells expressing VEGFR2^{R1051Q}. A-B: Seahorse Cell Mito Stress Test performed on Sk-Mel-31-VEGFR2^{WT} and Sk-Mel-31-VEGFR2^{R1051Q} cells. Cells were seeded in Seahorse XFe24 culture plates and incubated in CO_2 incubator at 37 °C. After 18 h, the medium was replaced with Agilent Seahorse XF base medium DMEM (pH 7.4) added with 10 mM Glc, 1 mM sodium pyruvate and 2 mM Gln. Cells were incubated for 1 h at 37 °C before performing Seahorse measurements. Oxygen consumption rate (OCR) was recorded over time before and after sequential addition of 1 µM oligomycin (Oligom), 0.5 µM FCCP and 1 µM Rotenone/Antimycin-A (Rot/Anti-A) (**A**) to enable the measurement of basal, ATP-linked, maximal and spare respiratory capacity, and proton leak (**B**). In parallel the extracellular acidification (ECAR) rate was recorded. Basal ECAR is shown. (**B**). At the end of the experiment, cells were lysed and total protein amount was measured for data normalization. Data are the mean ± SEM of three technical replicates in one representative experiment out of four independent measurements that provided similar results. **, $p < 0.01$, Student's *t*-test *versus* Sk-Mel-31-VEGFR2^{WT} **C:** bioluminescence-based real-time detection of ATP production in living Sk-Mel-31-VEGFR2^{WT} and Sk-Mel-31-VEGFR2^{R1051Q} cells. Data are shown as mean ± SEM of three independent experiments. *, $p < 0.05$, Student's *t*-test *versus* Sk-Mel-31-VEGFR2^{WT}. **D-E:** Seahorse measurement of basal (**D**) and maximal (**E**) OCR on Sk-Mel-31-VEGFR2^{WT} and Sk-Mel-31-VEGFR2^{R1051Q} cells previously treated for 18 h with increasing doses of Linifanib or vehicle (ctrl). Linifanib treatment did not significantly affect cell density. At the end of the experiment, cells were lysed and total protein amount was measured for data normalization. Data are shown as the average of normalized % of ctrl ± SEM of three independent experiments. *, $p < 0.05$, ****, $p < 0.001$, one-way ANOVA corrected by the Dunnett's multiple comparison test *versus* untreated cells. **F:** Western blot analysis of the indicated subunits of electron transport chain complexes on total Sk-Mel-31-VEGFR2^{WT} and Sk-Mel-31-VEGFR2^{R1051Q} cell lysates. GAPDH, loading control. **G:** cell proliferation in the presence of increasing doses of Antimycin-A. Data are shown as mean ± SEM of three independent experiments.

enrichment of the glycolysis pathway in Sk-Mel-31 cells expressing activated VEGFR2^{R1051Q}. Of note, the observed glycolysis activation suggests an increased flux of glucose 6-phosphate in the pentose phosphate pathway, providing cells with NADPH for the reductive anabolic processes and ribose 5-phosphate for nucleotides biosynthesis. Also, the augmented expression of *LDHA* paralleled by higher expression of *SLC16A3* (*MCT4,* the lactate shuttle) suggests that VEGFR2^{R1051Q} increases the channeling of pyruvate to lactate, with the consequence of a net increase in medium acidification (ECAR) and ATP production as a result of increased glycolysis. Increased glutaminolysis may also contribute to lactate increase in Sk-Mel-31 cells with VEGFR2^{R1051Q}, as suggested by the overexpression of liver type glutaminase (GLS2), the first enzyme required for Gln catabolism. The relevance of these molecular changes is supported by preclinical studies. *LDHA* has been proposed as a therapeutic target for lung cancer treatment, demonstrating that cancer-initiating cells are susceptible to its inhibition [37]. Similarly, we speculate that inhibition of *LDHA* may revert the "glycolytic" effects of aberrant VEGFR2 activation. However, mutated VEGFR2, despite being able to increase basal glycolysis, does not increase the glycolytic addiction of Sk-Mel-31 cells.

Sk-Mel-31 cells expressing VEGFR2^{R1051Q} exhibit also higher expression of various OXPHOS genes and a much higher mitochondrial respiration when compared to cells expressing wild-type VEGFR2. The specific inhibitory effect of the TKi Linifanib on the oxygen consumption of Sk-Mel-31-VEGFR2^{R1051Q} cells confirms that these metabolic changes directly depend on aberrant VEGFR2 signaling. Increasing evidence demonstrates that various cancers rely on OXPHOS [38]. In some cases, reliance on OXPHOS arises following targeted therapy and correlates with high aggressiveness, as it is the case for the blockade of the BRAF/MEK pathway in melanoma [39]. On these bases, the anti-tumor effects of various anti-OXPHOS approaches are currently being evaluated. However, preliminary observations indicate that antimycin A exerts a similar inhibitory effect on the proliferation of Sk-Mel-31 cells regardless if they express mutated or wild-type VEGFR2.

PCR array analysis showed for the first time a direct connection between VEGFR2 activation and FA metabolism. Indeed, several enzymes involved in FA beta-oxidation are overexpressed in Sk-Mel-31-VEGFR2^{R1051Q} cells, including *ACADS*, *ACAA2*, *ACAT2* and the

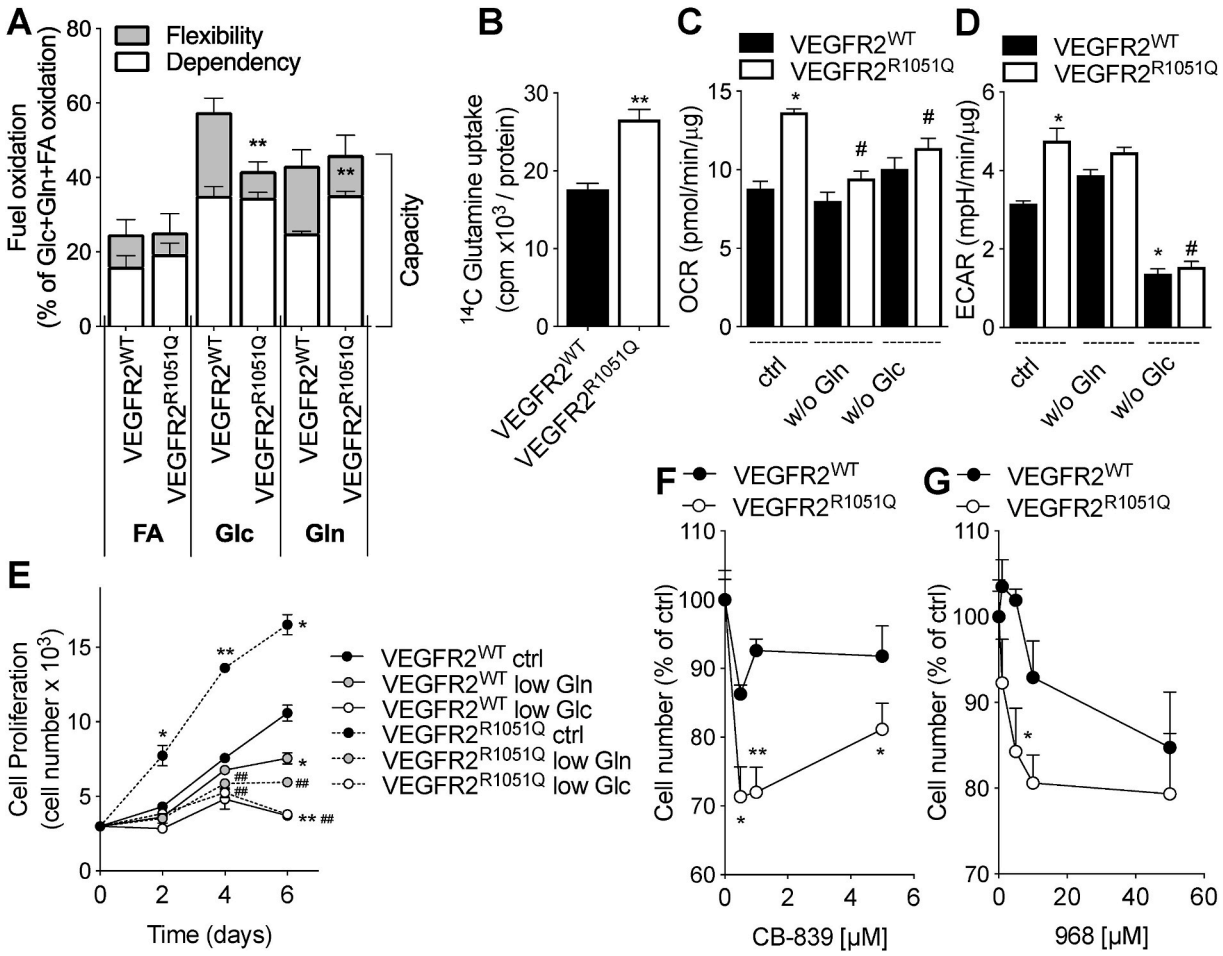

Fig. 4. Glutamine dependence in melanoma cells expressing VEGFR2^{R1051Q}. A: Seahorse Mito Fuel Flex Test performed on Sk-Mel-31-VEGFR2^{WT} and Sk-Mel-31-VEGFR^{2R1051Q} cells. Cells were seeded in Seahorse XFe24 culture plates and incubated in CO_2 incubator at 37 °C. After 18 h, the medium was replaced with Agilent Seahorse XF base medium DMEM (pH 7.4) added with 10 mM Glc, 1 mM sodium pyruvate and 2 mM Gln. Cells were incubated for 1 h at 37 °C before performing Seahorse measurements. OCR was measured over time before and after sequential addition of target inhibitors. Percentage of fuel oxidation [i.e. fuel (fatty acids, FA; glucose, Glc; glutamine, Gln) dependency and flexibility] was calculated using the Seahorse Report Generator. **B:** ^{14}C-Gln uptake in Sk-Mel-31-VEGFR2^{WT} and Sk-Mel-31-VEGFR2^{R1051Q} cells. **C-D:** Seahorse measurement of basal OCR and ECAR on Sk-Mel-31-VEGFR2^{WT} and Sk-Mel-31-VEGFR2^{R1051Q} cells in the presence (ctrl) (2 mM) or the absence of Gln or Glc. **E:** cell growth curve of Sk-Mel-31-VEGFR2^{WT} and Sk-Mel-31-VEGFR2^{R1051Q} cells cultured in low-Gln medium (0.2 mM), low Glc (1 mM) or left untreated (ctrl) (Gln 2 mM, Glc 11 mM). **F-G:** cell proliferation of Sk-Mel-31-VEGFR2^{WT} and Sk-Mel-31-VEGFR2^{R1051Q} cells cultured in the absence or the presence of increasing doses of 968 or CB-839 glutaminase inhibitors. Data are shown as the mean of three independent experiments ± SEM. *, $p < 0.05$, **, $p < 0.01$, Student's *t*-test *versus* Sk-Mel-31-VEGFR2^{WT}. #, $p < 0.05$, ##, $p < 0.01$ Student's *t*-test *versus* untreated (ctrl) Sk-Mel-31-VEGFR2^{R1051Q}.

carnitine-palmitoyl-transferase-1A and 2(*CPT1A/2*) which catalyze the addition of carnitine to activated FA, necessary to shuttle FA into mitochondria for β-oxidation. FA catabolism may increase in Sk-Mel-31-VEGFR2^{R1051Q} cells to meet an increased energy demand. Of note, the overexpression of CPT1A predisposes colon cancer cells to a tumor-promoting cross talk with adipocytes [40].

Metabolic dependencies on Gln and aspartate are increased in tumor cells to fuel anabolic processes to support growth [41]. Gln, besides providing nitrogen for the biosynthesis of nucleotides and amino acids, sustains the tricarboxylic acid cycle (TCA) and mitochondrial OXPHOS. In addition, Gln sustains lipids synthesis through the reductive carboxylation of α-ketoglutarate giving rise to anabolic citrate that, in turn, provides cytosolic acetyl-CoA for fatty acid assembly [42]. In this condition, the citrate shuttle could provide a significant contribution to NADPH production through malic enzyme, further sustaining the reductive anabolic pathways required for cancer proliferation. Our data highlighted that the expression of mutated VEGFR2^{R1051Q} increases the dependence on Gln to sustain cell respiration, possibly to produce ATP and to fuel the TCA cycle for biosynthetic purposes. In accordance, mutated VEGFR2 increases the uptake of Gln. To this regard, a recent study has described the anti-tumor effects in melanoma of the potent glutamine uptake inhibitor IMD-0354 further pointing to Gln as an interesting target in melanoma [43].

Gln also contributes to nucleotide biosynthesis and to the maintenance of redox balance [44]. Accordingly, VEGFR2^{R1051Q} modulates the expression of various enzymes of purine biosynthesis, including *GART*, *NME1*, *APRT*, *AMPD3*, *ADSS, ADSSL1, ATIC, PFAS* and *PPAT* (Supplementary Table 1). However, the role of activated VEGFR2^{R1051Q} in regulating purine and redox metabolism *via* Gln remains to be addressed.

Gln addiction is a hallmark of cancer cells, which often display increased Gln catabolism. We observed an increase in *GLS2* and aspartate aminotransferase (*GOT1*) expression, suggesting that an increased Gln catabolism occurs in Sk-Mel-31-VEGFR2^{R1051Q} cells when compared to control cells. Accordingly, Gln withdrawal from the culture medium markedly reduces the proliferation of melanoma cells expressing oncogenic VEGFR2^{R1051Q}. Of note, overexpression of *GOT1* in AML [45] and high *GOT1/GLUD1* ratio in KRAS mutated tumors are associated with poor prognosis [46]. High *GOT1/GLUD1* ratio couples Gln consumption to the synthesis of non-essential amino acids to promote biosynthesis

and TCA anaplerosis [46]. We can speculate that Sk-Mel-31--VEGFR2^{R1051Q} cells, in which *GLUD1* is downregulated, may use Gln in a similar way to fuel the TCA for biosynthetic purposes.

The understanding of metabolic reprogramming in cancer is key to identify druggable metabolic vulnerabilities. Gln addiction is a promising therapeutic target [47] and CB-839, an inhibitor of the kidney isoform of glutaminase (GLS1), has been evaluated in clinical trials ([48] clinicaltrials.gov, ID: NCT02071862). Also, targeting GLS2 with the pan-GLS 968 inhibitor blocks the growth of luminal subtype breast cancer [49]. Remarkably, Gln dependence has been shown to be the only metabolic defect to affect treatment and prognosis of cutaneous melanoma [50]. The selective effect of GLS inhibitors on the proliferation of Sk-Mel-31-VEGFR2^{R1051Q} cells supports the hypothesis that GLS may represent a therapeutic target alone or in combination with TKi also in tumors expressing VEGFR2^{R1051Q}. To our knowledge, this represents the first experimental evidence about a metabolic vulnerability of tumors with oncogenic activation of VEGFR2. Additional cellular models as well as *in vivo* experiments will help to confirm the translational potency of our findings.

In summary, here we describe for the first time that aberrant VEGFR2 signaling, consequent to R1051Q mutation, directly induces a reshaping of cell metabolism by increasing Gln uptake, usage, and dependence of melanoma cells. This study expands the list of RTKs (and mutations) which are worth attention in terms of potential predictors of response to metabolism-targeted therapies and point to Gln metabolism targeting as a promising strategy to treat tumors with mutated VEGFR2. Recently, we and others have shown that the R1051Q mutation recurs on similar residues across analogous RTKs [13,18]. Mutations clustered on corresponding residues across different proteins with similar function have been suggested to elicit similar biological effects on protein function [51,52]. On these bases, we anticipate that metabolic changes similar to those observed in VEGFR2^{R1051Q}-expressing cells may occur also in tumors harboring analogous RTK mutations, thus representing novel targets for the development of precision therapeutics in oncology.

Authors' contributions

Conceptualization, Methodology and Formal analysis: E.G., S.M, A. M. Investigation: E.G., M.C., C.R., M.B. Writing original draft: E.G., S.M. Writing reviewing and editing: E.M., M.P. Project administration: S.M. Funding acquisition: M.P., S.M.

Declaration of competing interest

All authors declare no Conflict of Interest.

Acknowledgements

This work was supported by grants from Associazione Italiana per la Ricerca sul Cancro (AIRC) to S.M. (IG17276), to A.M. (IG-22941) and to M.P. (IG 2019 Id.23116). E.G. was supported by Fondazione Italiana per la Ricerca sul Cancro (FIRC) and Fondazione Umberto Veronesi (FUV) Fellowships. M.B. was supported by Fondazione Pezcoller/SIC Prof. ssa De Gasperi Ronc. A.M. was supported by Fondazione Cassa di Risparmio di Firenze, Italy (MultiUser-19515). The authors are grateful to Prof. Kurt Ballmer-Hofer for helpful discussion and for having provided plasmids, and to Dr. Tiziana Schioppa for technical help.

Appendix A. Supplementary data

Supplementary data to this article can be found online at https://doi.org/10.1016/j.canlet.2021.03.007.

References

[1] Z. Du, C.M. Lovly, Mechanisms of receptor tyrosine kinase activation in cancer, Mol. Canc. 17 (2018) 58.
[2] E. Pupo, D. Avanzato, E. Middonti, F. Bussolino, L. Lanzetti, KRAS-driven metabolic rewiring reveals novel actionable targets in cancer, Front Oncol 9 (2019) 848.
[3] D. Hanahan, R.A. Weinberg, Hallmarks of cancer: the next generation, Cell 144 (2011) 646–674.
[4] P.S. Ward, C.B. Thompson, Signaling in control of cell growth and metabolism, Cold Spring Harb Perspect Biol 4 (2012) a006783.
[5] N. Jin, A. Bi, X. Lan, J. Xu, X. Wang, Y. Liu, T. Wang, S. Tang, H. Zeng, Z. Chen, M. Tan, J. Ai, H. Xie, T. Zhang, D. Liu, R. Huang, Y. Song, E.L. Leung, X. Yao, J. Ding, M. Geng, S.H. Lin, M. Huang, Identification of metabolic vulnerabilities of receptor tyrosine kinases-driven cancer, Nat. Commun. 10 (2019) 2701.
[6] L. Lian, X.L. Li, M.D. Xu, X.M. Li, M.Y. Wu, Y. Zhang, M. Tao, W. Li, X.M. Shen, C. Zhou, M. Jiang, VEGFR2 promotes tumorigenesis and metastasis in a pro-angiogenic-independent way in gastric cancer, BMC Canc. 19 (2019) 183.
[7] D. Zhao, C. Pan, J. Sun, C. Gilbert, K. Drews-Elger, D.J. Azzam, M. Picon-Ruiz, M. Kim, W. Ullmer, D. El-Ashry, C.J. Creighton, J.M. Slingerland, VEGF drives cancer-initiating stem cells through VEGFR-2/Stat3 signaling to upregulate Myc and Sox2, Oncogene 34 (2015) 3107–3119.
[8] G.G. Jinesh, G.C. Manyam, C.O. Mmeje, K.A. Baggerly, A.M. Kamat, Surface PD-L1, E-cadherin, CD24, and VEGFR2 as markers of epithelial cancer stem cells associated with rapid tumorigenesis, Sci. Rep. 7 (2017) 9602.
[9] J. Graells, A. Vinyals, A. Figueras, A. Llorens, A. Moreno, J. Marcoval, F. J. Gonzalez, A. Fabra, Overproduction of VEGF concomitantly expressed with its receptors promotes growth and survival of melanoma cells through MAPK and PI3K signaling, J. Invest. Dermatol. 123 (2004) 1151–1161.
[10] R. Masood, J. Cai, T. Zheng, D.L. Smith, D.R. Hinton, P.S. Gill, Vascular endothelial growth factor (VEGF) is an autocrine growth factor for VEGF receptor-positive human tumors, Blood 98 (2001) 1904–1913.
[11] I. Sher, S.A. Adham, J. Petrik, B.L. Coomber, Autocrine VEGF-A/KDR loop protects epithelial ovarian carcinoma cells from anoikis, Int. J. Canc. 124 (2009) 553–561.
[12] M. Miao, G. Deng, S. Luo, J. Zhou, L. Chen, J. Yang, J. He, J. Li, J. Yao, S. Tan, J. Tang, A phase II study of apatinib in patients with recurrent epithelial ovarian cancer, Gynecol. Oncol. 148 (2018) 286–290.
[13] E. Grillo, M. Corsini, C. Ravelli, M. di Somma, L. Zammataro, E. Monti, M. Presta, S. Mitola, A novel variant of VEGFR2 identified by a pan-cancer screening of recurrent somatic mutations in the catalytic domain of tyrosine kinase receptors enhances tumor growth and metastasis, Canc. Lett. 496 (2021) 84–92.
[14] R.A. Toledo, E. Garralda, M. Mitsi, T. Pons, J. Monsech, E. Vega, A. Otero, M. I. Albarran, N. Banos, Y. Duran, V. Bonilla, F. Sarno, M. Camacho-Artacho, T. Sanchez-Perez, S. Perea, R. Alvarez, A. De Martino, D. Lietha, C. Blanco-Aparicio, A. Cubillo, O. Dominguez, J.L. Martinez-Torrecuadrada, M. Hidalgo, Exome sequencing of plasma DNA portrays the mutation landscape of colorectal cancer and discovers mutated VEGFR2 receptors as modulators of antiangiogenic therapies, Clin. Canc. Res. 24 (2018) 3550–3559.
[15] C.R. Antonescu, A. Yoshida, T. Guo, N.E. Chang, L. Zhang, N.P. Agaram, L.X. Qin, M.F. Brennan, S. Singer, R.G. Maki, KDR activating mutations in human angiosarcomas are sensitive to specific kinase inhibitors, Canc. Res. 69 (2009) 7175–7179.
[16] A. Loaiza-Bonilla, C.E. Jensen, S. Shroff, E. Furth, P.A. Bonilla-Reyes, A.F. Deik, J. Morrissette, KDR mutation as a novel predictive biomarker of exceptional response to regorafenib in metastatic colorectal cancer, Cureus 8 (2016) e478.
[17] T.C. Knepper, M.L. Freeman, G.T. Gibney, H.L. McLeod, J.S. Russell, Clinical response to pazopanib in a patient with KDR-mutated metastatic basal cell carcinoma, JAMA Dermatol 153 (2017) 607–609.
[18] R.D. Kumar, R. Bose, Analysis of somatic mutations across the kinome reveals loss-of-function mutations in multiple cancer types, Sci. Rep. 7 (2017) 6418.
[19] F. Baenke, B. Chaneton, M. Smith, N. Van Den Broek, K. Hogan, H. Tang, A. Viros, M. Martin, L. Galbraith, M.R. Girotti, N. Dhomen, E. Gottlieb, R. Marais, Resistance to BRAF inhibitors induces glutamine dependency in melanoma cells, Mol Oncol 10 (2016) 73–84.
[20] R. Ronca, G.C. Ghedini, F. Maccarinelli, A. Sacco, S.L. Locatelli, E. Foglio, S. Taranto, E. Grillo, S. Matarazzo, R. Castelli, G. Paganini, V. Desantis, N. Cattane, A. Cattaneo, M. Mor, C. Carlo-Stella, A. Belotti, A.M. Roccaro, M. Presta, A. Giacomini, FGF trapping inhibits multiple myeloma growth through c-myc degradation-induced mitochondrial oxidative stress, Canc. Res. 80 (2020) 2340–2354.
[21] M. Di Somma, W. Schaafsma, E. Grillo, M. Vliora, E. Dakou, M. Corsini, C. Ravelli, R. Ronca, P. Sakellariou, J. Vanparijs, B. Castro, S. Mitola, Natural histogel-based bio-scaffolds for sustaining angiogenesis in beige adipose tissue, Cells (2019) 8.
[22] E.Y. Chen, C.M. Tan, Y. Kou, Q. Duan, Z. Wang, G.V. Meirelles, N.R. Clark, A. Ma'ayan, Enrichr, Interactive and collaborative HTML5 gene list enrichment analysis tool, BMC Bioinf. 14 (2013) 128.
[23] M.V. Kuleshov, M.R. Jones, A.D. Rouillard, N.F. Fernandez, Q. Duan, Z. Wang, S. Koplev, S.L. Jenkins, K.M. Jagodnik, A. Lachmann, M.G. McDermott, C. D. Monteiro, G.W. Gundersen, A. Ma'ayan, Enrichr: a comprehensive gene set enrichment analysis web server 2016 update, Nucleic Acids Res. 44 (2016) W90–W97.
[24] S. Matarazzo, L. Melocchi, S. Rezzola, E. Grillo, F. Maccarinelli, A. Giacomini, M. Turati, S. Taranto, L. Zammataro, M. Cerasuolo, M. Bugatti, W. Vermi, M. Presta, R. Ronca, Long Pentraxin-3 Follows and Modulates Bladder Cancer Progression, Cancers (Basel), 2019, p. 11.

[25] M. Bacci, N. Lorito, L. Ippolito, M. Ramazzotti, S. Luti, S. Romagnoli, M. Parri, F. Bianchini, F. Cappellesso, F. Virga, Q. Gao, B.M. Simoes, E. Marangoni, L. A. Martin, G. Comito, M. Ferracin, E. Giannoni, M. Mazzone, P. Chiarugi, A. Morandi, Reprogramming of amino acid transporters to support aspartate and glutamate dependency sustains endocrine resistance in breast cancer, Cell Rep. 28 (2019) 104–118 e8.
[26] E.C. Lien, C.A. Lyssiotis, L.C. Cantley, Metabolic reprogramming by the PI3K-Akt-mTOR pathway in cancer, Recent Results Canc. Res. 207 (2016) 39–72.
[27] M.G. Vander Heiden, R.J. DeBerardinis, Understanding the intersections between metabolism and cancer biology, Cell 168 (2017) 657–669.
[28] R. Shiratori, K. Furuichi, M. Yamaguchi, N. Miyazaki, H. Aoki, H. Chibana, K. Ito, S. Aoki, Glycolytic suppression dramatically changes the intracellular metabolic profile of multiple cancer cell lines in a mitochondrial metabolism-dependent manner, Sci. Rep. 9 (2019) 18699.
[29] L. Chen, X. Cheng, W. Tu, Z. Qi, H. Li, F. Liu, Y. Yang, Z. Zhang, Z. Wang, Apatinib inhibits glycolysis by suppressing the VEGFR2/AKT1/SOX5/GLUT4 signaling pathway in ovarian cancer cells, Cell. Oncol. 42 (2019) 679–690.
[30] Q. Huang, S. Li, X. Hu, M. Sun, Q. Wu, H. Dai, Y. Tan, F. Sun, C. Wang, X. Rong, W. Liao, J. Peng, J. Xiao, L. Huang, J. Wang, B. Liang, K. Lin, Y. Liu, M. Shi, Shear stress activates ATOH8 via autocrine VEGF promoting glycolysis dependent-survival of colorectal cancer cells in the circulation, J. Exp. Clin. Canc. Res. 39 (2020) 25.
[31] S. Nobrega-Pereira, F. Caiado, T. Carvalho, I. Matias, G. Graca, L.G. Goncalves, B. Silva-Santos, H. Norell, S. Dias, VEGFR2-Mediated reprogramming of mitochondrial metabolism regulates the sensitivity of acute myeloid leukemia to chemotherapy, Canc. Res. 78 (2018) 731–741.
[32] G. Hoxhaj, B.D. Manning, The PI3K-AKT network at the interface of oncogenic signalling and cancer metabolism, Nat. Rev. Canc. 20 (2020) 74–88.
[33] R.M. Slominski, M.A. Zmijewski, A.T. Slominski, The role of melanin pigment in melanoma, Exp. Dermatol. 24 (2015) 258–259.
[34] Y.T. Chen, E. Stockert, A. Jungbluth, S. Tsang, K.A. Coplan, M.J. Scanlan, L.J. Old, Serological analysis of Melan-A(MART-1), a melanocyte-specific protein homogeneously expressed in human melanomas, Proc. Natl. Acad. Sci. U. S. A. 93 (1996) 5915–5919.
[35] K. De Bock, M. Georgiadou, S. Schoors, A. Kuchnio, B.W. Wong, A.R. Cantelmo, A. Quaegebeur, B. Ghesquiere, S. Cauwenberghs, G. Eelen, L.K. Phng, I. Betz, B. Tembuyser, K. Brepoels, J. Welti, I. Geudens, I. Segura, B. Cruys, F. Bifari, I. Decimo, R. Blanco, S. Wyns, J. Vangindertael, S. Rocha, R.T. Collins, S. Munck, D. Daelemans, H. Imamura, R. Devlieger, M. Rider, P.P. Van Veldhoven, F. Schuit, R. Bartrons, J. Hofkens, P. Fraisl, S. Telang, R.J. Deberardinis, L. Schoonjans, S. Vinckier, J. Chesney, H. Gerhardt, M. Dewerchin, P. Carmeliet, Role of PFKFB3-driven glycolysis in vessel sprouting, Cell 154 (2013) 651–663.
[36] W.L. Yeh, C.J. Lin, W.M. Fu, Enhancement of glucose transporter expression of brain endothelial cells by vascular endothelial growth factor derived from glioma exposed to hypoxia, Mol. Pharmacol. 73 (2008) 170–177.
[37] H. Xie, J. Hanai, J.G. Ren, L. Kats, K. Burgess, P. Bhargava, S. Signoretti, J. Billiard, K.J. Duffy, A. Grant, X. Wang, P.K. Lorkiewicz, S. Schatzman, M. Bousamra 2nd, A. N. Lane, R.M. Higashi, T.W. Fan, P.P. Pandolfi, V.P. Sukhatme, P. Seth, Targeting lactate dehydrogenase–a inhibits tumorigenesis and tumor progression in mouse models of lung cancer and impacts tumor-initiating cells, Cell Metabol. 19 (2014) 795–809.
[38] R.J. DeBerardinis, N.S. Chandel, Fundamentals of cancer metabolism, Sci Adv 2 (2016), e1600200.
[39] V. Audrito, A. Manago, F. Gaudino, S. Deaglio, Targeting metabolic reprogramming in metastatic melanoma: the key role of nicotinamide phosphoribosyltransferase (NAMPT), Semin. Cell Dev. Biol. 98 (2020) 192–201.
[40] X. Xiong, Y.A. Wen, R. Fairchild, Y.Y. Zaytseva, H.L. Weiss, B.M. Evers, T. Gao, Upregulation of CPT1A is essential for the tumor-promoting effect of adipocytes in colon cancer, Cell Death Dis. 11 (2020) 736.
[41] J. Son, C.A. Lyssiotis, H. Ying, X. Wang, S. Hua, M. Ligorio, R.M. Perera, C. R. Ferrone, E. Mullarky, N. Shyh-Chang, Y. Kang, J.B. Fleming, N. Bardeesy, J. M. Asara, M.C. Haigis, R.A. DePinho, L.C. Cantley, A.C. Kimmelman, Glutamine supports pancreatic cancer growth through a KRAS-regulated metabolic pathway, Nature 496 (2013) 101–105.
[42] N. Koundouros, G. Poulogiannis, Reprogramming of fatty acid metabolism in cancer, Br. J. Canc. 122 (2020) 4–22.
[43] Y. Feng, G. Pathria, S. Heynen-Genel, M.R. Jackson, B. James, J. Yin, D.A. Scott, Z. A. Ronai, Identification and characterization of IMD-0354 as a glutamine carrier protein inhibitor in melanoma, Mol. Canc. Therapeut. (2021).
[44] J. Zhang, N.N. Pavlova, C.B. Thompson, Cancer cell metabolism: the essential role of the nonessential amino acid, glutamine, EMBO J. 36 (2017) 1302–1315.
[45] Z. Cheng, Y. Dai, T. Zeng, Y. Liu, L. Cui, T. Qian, C. Si, W. Huang, Y. Pang, X. Ye, J. Shi, L. Fu, Upregulation of glutamic-oxaloacetic transaminase 1 predicts poor prognosis in acute myeloid leukemia, Front Oncol 10 (2020) 379.
[46] G. Chakrabarti, Z.R. Moore, X. Luo, M. Ilcheva, A. Ali, M. Padanad, Y. Zhou, Y. Xie, S. Burma, P.P. Scaglioni, L.C. Cantley, R.J. DeBerardinis, A.C. Kimmelman, C. A. Lyssiotis, D.A. Boothman, Targeting glutamine metabolism sensitizes pancreatic cancer to PARP-driven metabolic catastrophe induced by ss-lapachone, Canc. Metabol. 3 (2015) 12.
[47] J.B. Wang, J.W. Erickson, R. Fuji, S. Ramachandran, P. Gao, R. Dinavahi, K. F. Wilson, A.L. Ambrosio, S.M. Dias, C.V. Dang, R.A. Cerione, Targeting mitochondrial glutaminase activity inhibits oncogenic transformation, Canc. Cell 18 (2010) 207–219.
[48] M.I. Gross, S.D. Demo, J.B. Dennison, L. Chen, T. Chernov-Rogan, B. Goyal, J. R. Janes, G.J. Laidig, E.R. Lewis, J. Li, A.L. Mackinnon, F. Parlati, M.L. Rodriguez, P.J. Shwonek, E.B. Sjogren, T.F. Stanton, T. Wang, J. Yang, F. Zhao, M.K. Bennett, Antitumor activity of the glutaminase inhibitor CB-839 in triple-negative breast cancer, Mol. Canc. Therapeut. 13 (2014) 890–901.
[49] M.J. Lukey, A.A. Cluntun, W.P. Katt, M.J. Lin, J.E. Druso, S. Ramachandran, J. W. Erickson, H.H. Le, Z.E. Wang, B. Blank, K.S. Greene, R.A. Cerione, Liver-type glutaminase GLS2 is a druggable metabolic node in luminal-subtype breast cancer, Cell Rep. 29 (2019) 76–88 e77.
[50] K. Chen, H. Liu, Z. Liu, W. Bloomer, C.I. Amos, J.E. Lee, X. Li, H. Nan, Q. Wei, Genetic variants in glutamine metabolic pathway genes predict cutaneous melanoma-specific survival, Mol. Carcinog. 58 (2019) 2091–2103.
[51] M.L. Miller, E. Reznik, N.P. Gauthier, B.A. Aksoy, A. Korkut, J. Gao, G. Ciriello, N. Schultz, C. Sander, Pan-cancer analysis of mutation hotspots in protein domains, Cell Syst 1 (2015) 197–209.
[52] G.E. Melloni, S. de Pretis, L. Riva, M. Pelizzola, A. Ceol, J. Costanza, H. Muller, L. Zammataro, LowMACA: exploiting protein family analysis for the identification of rare driver mutations in cancer, BMC Bioinf. 17 (2016) 80.